Swift heavy ion tracks in nanocrystalline Y$_4$Al$_2$O$_9$

Anel Ibrayeva [a,b,c,*], Alisher Mutali [a,b,d], Jacques O'Connell [c], Arno Janse van Vuuren [c], Ekaterina Korneeva [a,e], Alexander Sohatsky [a], Ruslan Rymzhanov [a,b], Vladimir Skuratov [a,f,g], Liudmila Alekseeva [h], Igor Ivanov [b]

[a] Flerov Laboratory of Nuclear Research, Joint Institute for Nuclear Research, Dubna, Russia
[b] Institute of Nuclear Physics, Almaty, Kazakhstan
[c] Centre for HRTEM, Nelson Mandela University, Port Elizabeth, South Africa
[d] L.N. Gumilyov Eurasian National University, Nur-Sultan, Kazakhstan
[e] National University of Science and Technology NUST-MISiS, Moscow, Russia
[f] National Research Nuclear University MEPhI, Moscow, Russia
[g] Dubna State University, Dubna, Russia
[h] Physico-Technical Research Institute, Lobachevsky State University of Nizhny Novgorod, Nizhny Novgorod, Russia

ARTICLE INFO

ABSTRACT

We report the first results of a TEM study of structural changes induced by high energy xenon and bismuth ions in Y$_4$Al$_2$O$_9$ nanoparticles (10 to 100 nm grain size) in the range of electronic stopping powers $6 \div 35$ keV/nm. It was found that swift Xe an Bi ion irradiation, starting from threshold energy loss ~ 8 keV/nm, leads to the formation of continuous amorphous latent tracks, while discontinuous tracks are observed at ~ 6 keV/nm. No effect of grain size on the ion track parameters was observed for all specific ionizing energy losses used in experiments.

1. Introduction

Radiation tolerance of nanocrystalline oxide ceramics against swift heavy ion (SHI) irradiation has been extensively studied in recent years (for example, [1–8]). In addition to practical interest related to the simulation of fission fragment impacts, there are also fundamental issues concerned with the role of confinement of excited electrons in structural changes. In particular, it is of considerable interest to investigate how the localization of energy, deposited via electronic excitations, affects latent track or associated damage formation processes in nanograins. Contrary to conventional irradiation demonstrating an enhanced radiation resistance due to high grain boundary densities, there are examples that high energy heavy ion exposure may reduce the stability of nanocrystalline materials in comparison with microcrystalline ones, as was reported in [2,5]. Most available data were obtained using XRD and Raman techniques and targets as nanopowders pressed into pellets [1–8]. As a result, these methods provided information averaged over a large number of grains. The only technique with sufficient spatial resolution to examine the structure of isolated nanoparticles is transmission electron microscopy (TEM). However, very few studies are available in the literature where TEM was used for the characterization of SHI induced effects in individual nano-oxides or their small agglomerates [9–20]. It should be noted that in some works TEM was utilized to determine crystallite/grain size prior to SHI irradiation (for example, [5]).

Latent tracks of 4.6 MeV/amu Pb ions as cylindrical holes were reported in tin oxide nanopowder deposited on copper grids and irradiated to a fluence of 3×10^{11} cm^{-2} [9]. The radii of such tracks corresponded to the theoretical vaporized radius in the framework of the thermal spike model (TSM). At higher fluences, above 2×10^{12} cm^{-2}, TEM observations have revealed that the largest grains with size ~ 150 nm split into ~ 20 nm sized nanodomains while the smallest ones disappear [10]. The TSM has predicted a critical radius of 8 nm for completely evaporated grains. The formation of nanodomains was ascribed to a pressure effect via accumulation of a number of pressurized zones (due to ion tracks) until a critical value is reached [10]. High energy Ar (6.7 MeV/amu), Cd (9.9 MeV/amu), Ta (6.04 MeV/amu), Pb (4.06 MeV/amu), and U (3.4 MeV/amu) ion irradiated SnO$_2$ nanometric powders have been studied
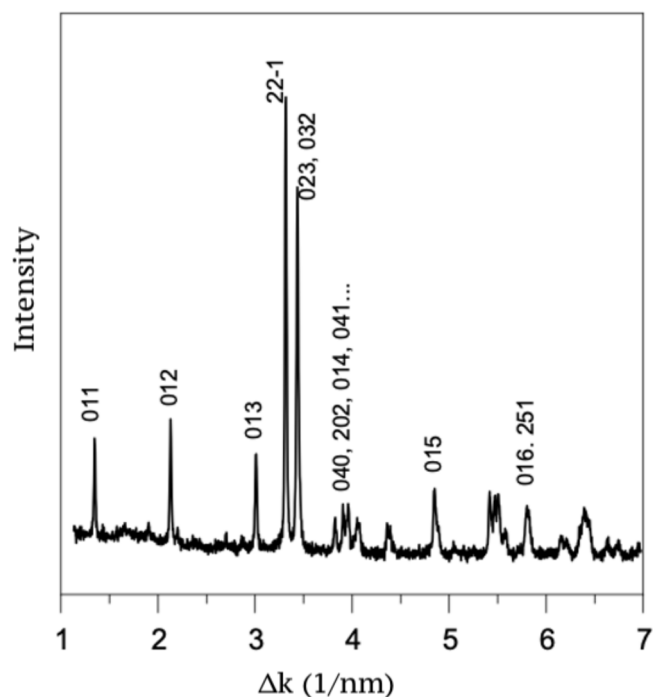
Fig. 1. XRD spectrum collected from pristine YAM nanopowder.

using high resolution TEM in [11]. It was found that all ions except Ar, induce cylindrical tracks. Ta, Pb and U ions with the highest electronic stopping power created cylindrical holes, while in the case of Cd ion irradiation, a crystal-like contrast remained in the core track. Cylindrical holes correspond to a local zone where the maximum temperature calculated using the TSM exceeds the boiling point.

High resolution TEM examination of nanocrystalline Y_2O_3 irradiated with 120 MeV Ag ions to a fluence of 3×10^{13} cm^{-2} has revealed the absence of amorphization but cubic to monoclinic phase transition [12]. It was also found that the average grain size changed from 25 to 17 nm.

The SHI irradiation induced structural transformations in Y-Ti nano-oxides embedded into metallic (ferritic) matrices, oxide dispersion strengthened (ODS) alloys, have been studied in [13–20]. Amorphous latent tracks were observed in Y_2TiO_5 and $Y_2Ti_2O_7$ nanoparticles with size variance from tens to hundreds of nm. The most detailed analysis was done for $Y_2Ti_2O_7$ pyrochlore nanoparticles in EP450 ODS steel irradiated by 1.2 MeV/amu xenon, krypton and argon ions in the range of electronic stopping powers 3.6–24.3 keV/nm [17]. It was found that track diameters are in the range 3 to 7 nm for electronic stopping powers in the range 10 to 24 keV/nm. The threshold ionization energy loss for track formation was estimated to be between 7.4 keV/nm and 9.7 keV/nm. Another finding was that SHI irradiation in the track overlapping regime (1.5×10^{13} 710 MeV Bi/cm^2) led to complete amorphization of

Y-Ti nano-oxides.

No latent tracks have been revealed in $Y_4Al_2O_9$ (YAM) particles in KP4 alloy irradiated with 710 MeV Bi ions as well as no amorphization of $Y_4Al_2O_9$ oxides was observed after exposure at the same Bi ion fluences, up to 1.5×10^{13} cm^{-2} [20]. Small $Y_4Al_2O_9$ oxides (~5 nm), remained crystalline and only subsurface (interfacial) regions in large (~20 nm) particles were amorphized. 167 MeV Xe ion irradiation at fluences of 10^{14} cm^{-2} and 1.5×10^{15} cm^{-2} resulted in amorphization of small $Y_4Al_2O_9$ particles while the amorphous bodies of large particles were found to contain small crystalline inclusions [20]. Such enhanced radiation stability of Y-Al-O nanoparticles in metallic matrices in comparison with Y-Ti nano-oxides motivates further research of YAM involving new irradiation conditions. It should be noted that no data about SHI induced defects in both single and polycrystalline YAM as well as nanocrystalline, except of those mentioned above, are known from the literature. The aim of this work is TEM examination of structural changes in individual YAM nano-oxides (not in a metallic matrix) irradiated with high energy Bi and Xe ions in a wide range of electronic stopping powers.

2. Materials and methods

Nanocrystalline $Y_4Al_2O_9$ powder (grain size 10 to 100 nm and average grain size 43.4 ± 0.7 nm) was synthesized by means of the citrate–nitrate sol–gel combustion. For this, $Y(NO_3)_3$ (yttrium(III) nitrate hexahydrate, 99.99%) and $Al(NO_3)_3$ (aluminium(III) nitrate nonahydrate, 99%) precursors were added to distilled water in a ratio 2:1. The citric acid (CA) solution was added to the nitrate mixture in the molar ratio 1 : 1 (NO_3- : CA). The resulting mixture was evaporated at 130 °C with constant stirring until a thick gel was formed, which was then annealed at 350 °C for 2 h. The resulting powder was heated to 1000 °C at a rate of 5 °C/min and annealed for 1 h. The powder was sonicated with ethanol and dispersed on TEM copper grids, which were directly used for irradiation experiments and TEM examination. The monoclinic phase of pristine specimens was verified by XRD measurements (Fig. 1). Peak positions shown in Fig. 1 agree with those known from the literature [21].

The specimens were irradiated with 156 MeV Xe, 230 MeV Xe and 714 MeV Bi ions to a fluence of 5×10^{11} cm^{-2} at the IC-100, U-400 and DC-60 cyclotrons at FLNR JINR (Dubna, Russia) and Astana Branch of Institute of Nuclear Physics (Nur-Sultan, Kazakhstan). Ion beam homogeneity over the irradiated specimen surface was controlled using beam scanning in the horizontal and vertical directions and was better than 10%. Average Bi and Xe ion fluxes were less than 10^8 cm^{-2}s^{-1} to avoid any significant heating of the specimens. To widen the ion energy range, Al degraders of varying thicknesses have been used. Energy spreading (average values and standard deviation) after passing through the degraders as well as electronic energy losses, S_e, was calculated using SRIM code.

Structural examination was performed using Talos™ F200i S/TEM and JEOL ARM-200F TEM operating at 200 kV. TEM analysis done prior
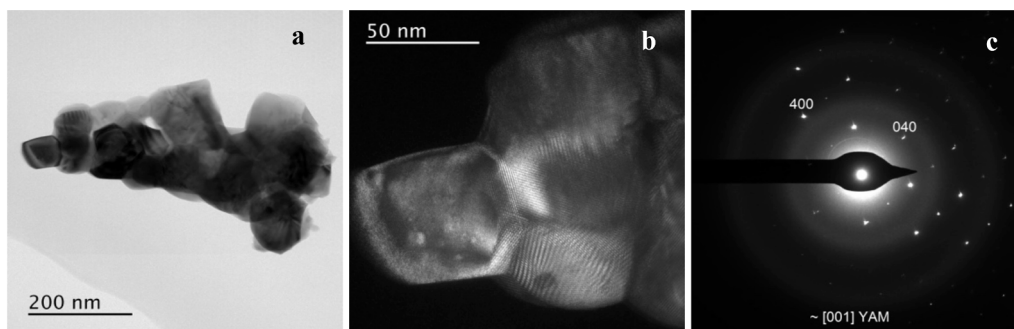

Fig. 2. BF (a) and DF (b) TEM images of YAM nanoparticles. (c) – SAED pattern from individual grain prior to irradiation.
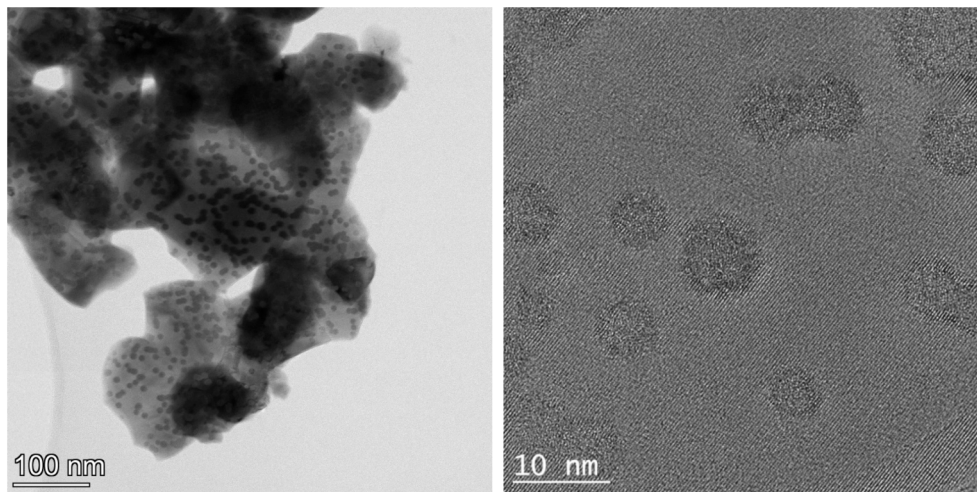
Fig. 3. BF TEM (left) and HRTEM (right) images of nc-YAM irradiated with 230 MeV Xe ions.
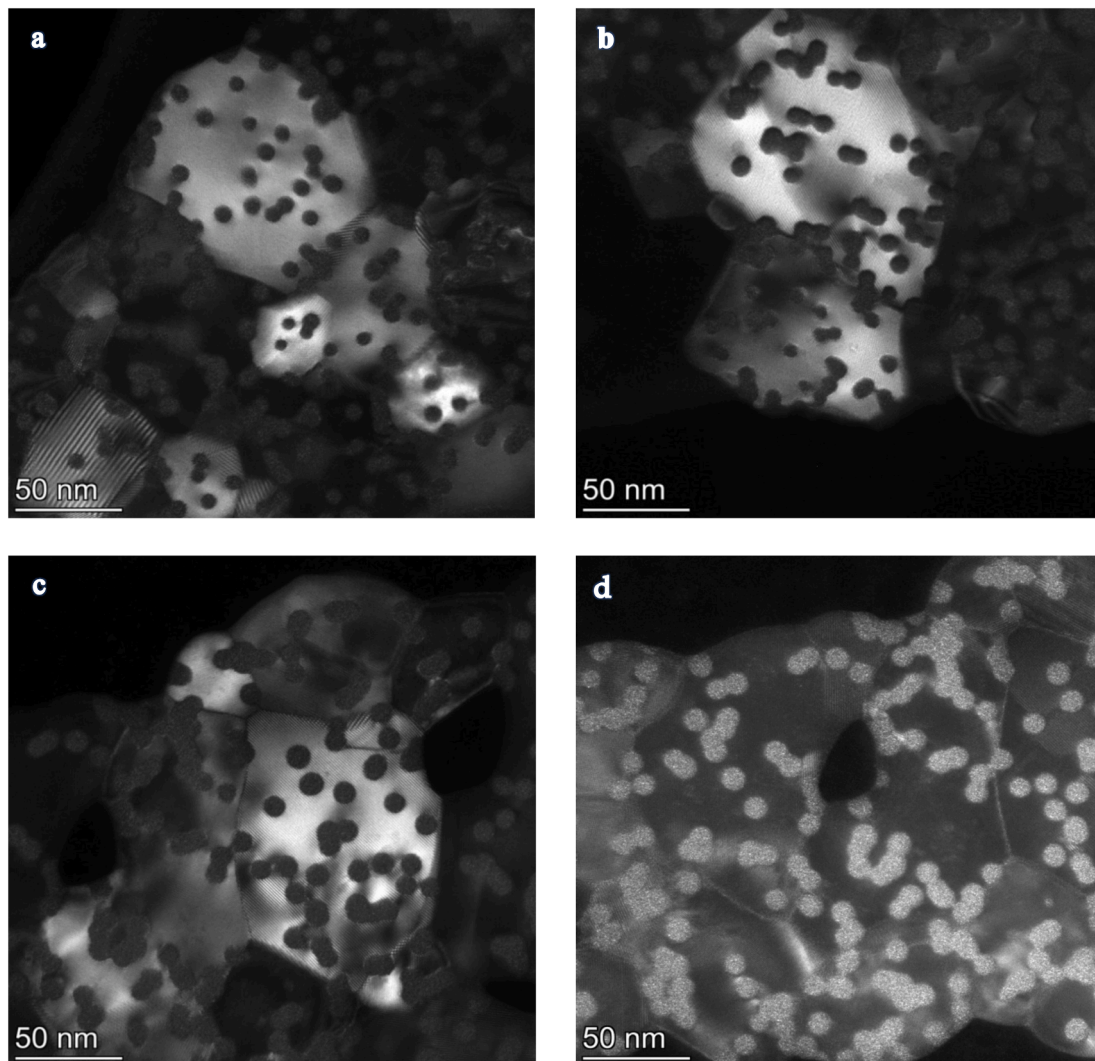

Fig. 4. DF TEM images of nc-YAM irradiated with (a) 156 MeV Xe, (b) 230 MeV Xe, (c) 714 MeV Bi ions. (d) – DF image of 230 MeV Xe ion induced tracks in the non-reflective position.

Table 1

Details of irradiation parameters and track measurements for nanocrystalline $Y_4Al_2O_9$.

Ion, energy	Al degrader, μm	Ion energy, MeV/amu	S_e, keV/nm	Track radius, nm
Bi, 714 MeV	no	3.4	35.3 ± 0.2	4.8 ± 0.3
	14	1.7	30.9 ± 0.4	5.5 ± 0.2
	17.4	1.4	28.6 ± 0.5	5.3 ± 0.3
	19.2	1.2	27.3 ± 0.5	5.1 ± 0.2
	23.2	0.8	23.5 ± 0.5	4.7 ± 0.3
	27	0.5	19.1 ± 0.5	3.4 ± 0.3
	28.7	0.4	16.7 ± 0.6	2.7 ± 0.4
	34.7	0.1	7.8 ± 0.6	no tracks
Xe, 230 MeV	no	1.8	22.5 ± 0.4	3.8 ± 0.4
	8	0.8	18.3 ± 0.3	3.6 ± 0.3
	9.6	0.7	17.1 ± 0.6	3.9 ± 0.4
	11.7	0.5	14.9 ± 0.6	3.4 ± 0.3
	14	0.3	11.8 ± 0.4	3.0 ± 0.4
	16	0.2	8.4 ± 0.6	2.8 ± 0.5
	17.4	0.1	6.2 ± 0.5	$0 \div 2$
Xe, 156 MeV	no	1.2	20.4 ± 0.3	3.6 ± 0.3
	7.5	0.4	13.8 ± 0.3	4.0 ± 0.5
	10	0.3	11.6 ± 0.4	3.3 ± 0.4

Fig. 5. Track radius as a function of electron energy loss.

power is due to the energy dispersion of the incident ion beam after passing through the aluminum foil.

4. Discussion

Ion track radii vs specific ionizing energy losses are given in Fig. 5. Interest in such plots stem from the fact that the experimentally determined track sizes and threshold energy loss S_{et} are the only parameters that can be used for verification of existing theoretical models of track formation.

An evident problem in finding the correct S_{et} value is the track morphology at low (near threshold) stopping powers. Fig. 6 shows tracks in nc-YAM produced by 1.8 and 0.1 MeV/amu energy xenon ions with corresponding $S_e = 22.5$ and 6.2 keV/nm, respectively. Despite detection of "TEM visible" tracks, it is impossible to determine their size at $\sim$ 6 keV/nm scattered in the range $0 \div 2$ nm. We suggest that lower density of tracks in comparison with ion fluence and irregular shape may indicate that tracks are discontinuous at this energy loss. The transition from amorphous continuous to discontinuous tracks is quite common for energy losses near the threshold of track formation [22,23]. Therefore, it seems reasonable to speak about two different thresholds for both continuous and discontinuous tracks. According to our data the upper limit for discontinuous track formation in nc-YAM is no more than 6.2 keV/nm. As for continuous tracks, we have contradictory results. As shown in Fig. 5, no tracks were registered in 0.1 MeV/amu Bi ion irradiated specimens contrary to Xe ion irradiation at a similar ($\sim$7–8 keV/nm) energy loss. Lower track radius for Bi ions in comparison with Xe ions was also observed at $S_e \sim 17$ keV/nm. It should be noted that despite different Xe and Bi ion velocities, this discrepancy cannot be due to the velocity effect which predicts a bigger track size at lower ion velocity for the same stopping power (for example, [22]) since the trend shown by our data (see Fig. 5 and Appendix B) is opposite that of the velocity effect.

A possible effect of the nuclear energy loss, S_n, should be ruled out of consideration in view of its negligible contribution in total stopping power. Actually, the nuclear energy loss may play an important role in the track formation when its level is comparable or higher than electronic energy loss, as demonstrated in a TEM study of latent track parameters in amorphous silicon nitride films irradiated with high energy monoatomic ions and fullerenes [24]. One more process affecting the final track size is recrystallization of distorted regions after initial excitation [25]. However, the amorphous nature of ion tracks suggests that no significant recrystallization occurs in YAM as an amorphizable
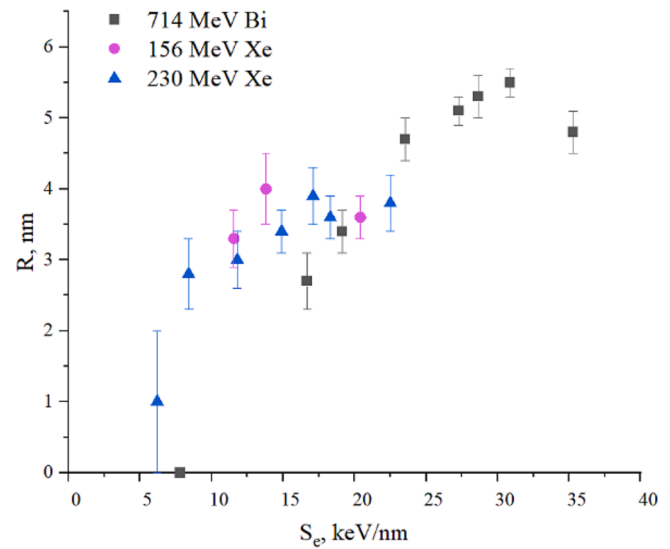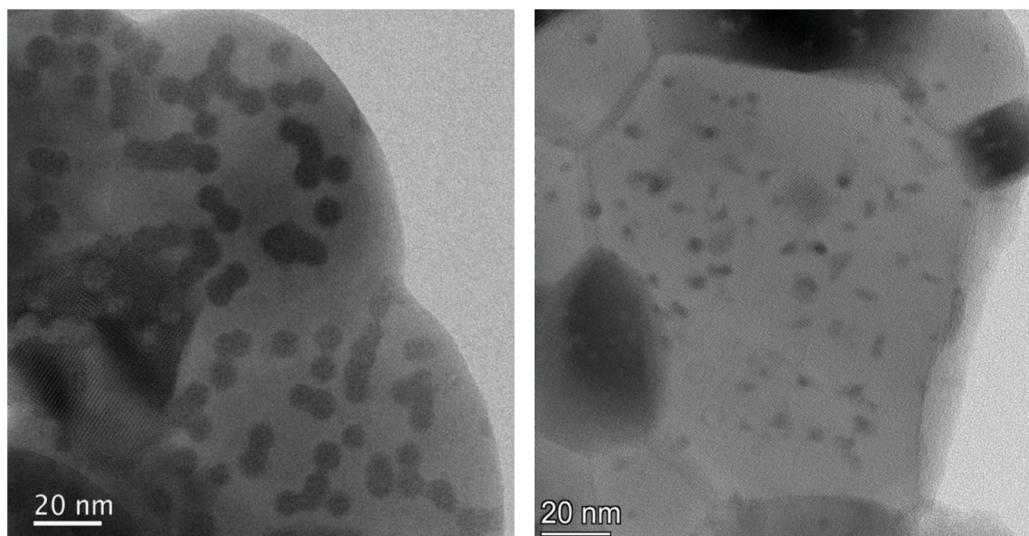
to irradiation has revealed that YAM nanoparticles are composed of individual single crystalline grains as follows from bright-field (BF) and dark-field (DF) images shown in Fig. 2. The SAED pattern taken from an individual grain confirms its monoclinic phase.

3. Results

It was found that high energy Xe and Bi ions, induce latent tracks in nanocrystalline YAM (nc-YAM) particles when the electronic stopping power exceeds some threshold value as shown in Fig. 3. The areal track density was equal to the fluence 5×10^{11} cm^{-2} within the accuracy of ion fluence measurements (15%) for all specimens except those that were irradiated close to the threshold electronic stopping power ($\sim$6 keV/nm for 15.7 MeV Xe). This implies that any ion hit results in track formation. TEM analysis of a large number of particles has shown that track sizes at a fixed electronic stopping power are very similar in small ($\sim$20 nm) and large ($\sim$100 nm) grains (a TEM image is presented as an example in Appendix A).

The morphology of tracks (cylindrical regions of amorphous material along the ion path) was determined using DF TEM images, some of which are shown in Fig. 4a–c. Electron diffraction from amorphous Y-Al-O oxide is much weaker than diffraction from crystalline YAM grains in reflecting positions; that is why the amorphous material of tracks in such grains is not visible in DF images (Fig. 4a–c). In contrast, amorphous tracks are seen in the DF image of the grains in the non-reflective position (Fig. 4d). An inhomogeneous substance of ion tracks is seen as regions consisting of many small light dots, thus clearly demonstrating their cluster, so-called X-ray amorphous structure.

Table 1 summarizes track sizes deduced from analysis of TEM micrographs. Bi and Xe ion energies, specific ionizing energy loss and thickness of Al degraders are also given. S_e values were calculated assuming a density of 4.45 g/cm^3 for $Y_4Al_2O_9$). The error in the stopping

Fig. 6. BF TEM images of nc-YAM irradiated with 230 MeV (left) and 15.7 MeV (right) Xe ions.

material. The reason for the difference in Xe and Bi ion track radii at near threshold stopping powers requires further research with the possible involvement of another ion species. At present, the threshold electronic energy loss for continuous track formation in nc-YAM can be estimated to be ~ 8 keV/nm.

Since no other data about SHI induced structural transformations in YAM are known from the literature, we cannot compare track parameters in the same nano- and poly/single crystalline material. Considering data available for yttrium aluminum garnet (YAG) $Y_3Al_5O_{12}$ single crystals, (similar to YAM by composition and thermal properties Y-Al oxide), one should note the similarity in track sizes [26,27] and in track formation threshold of approximately 6 keV/ nm, determined by extrapolation of the thermal spike calculations [26]. This may imply that if a significant effect of electron confinement does exists for small grain sizes, the critical size for the onset of such effects should be below 20 nm which were the smallest grains studied in this work.

5. Conclusions

Latent tracks induced by high energy xenon and bismuth ions form in nanocrystalline YAM and can be imaged by TEM. This is in contrast to the high radiation stability under SHI impact of these nanocrystals included in a metallic matrix [20]. The threshold electronic stopping power was found to be about 8 keV/nm and not more than 6.2 keV/nm for the formation of continuous and discontinuous tracks respectively. Unfortunately, different results corresponding to track parameters at lowest S_e values of Xe and Bi ion irradiation could not be explained properly within this investigation and requires additional studies.

CRediT authorship contribution statement

Anel Ibrayeva: Conceptualization, Investigation, Writing – original draft, Writing – review & editing, Supervision, Funding acquisition. **Alisher Mutali:** Methodology, Investigation, Visualization. **Jacques O'Connell:** Validation, Investigation, Writing – review & editing. **Arno Janse van Vuuren:** Validation, Investigation. **Ekaterina Korneeva:** Methodology, Investigation. **Alexander Sohatsky:** Validation, Investigation, Resources, Visualization. **Ruslan Rymzhanov:** Formal analysis, Data curation. **Vladimir Skuratov:** Conceptualization, Resources, Writing – review & editing, Supervision, Project administration, Funding acquisition. **Liudmila Alekseeva:** Methodology. **Igor Ivanov:** Investigation.

Declaration of Competing Interest

The authors declare that they have no known competing financial interests or personal relationships that could have appeared to influence the work reported in this paper.

Appendix A. Supplementary data

Supplementary data to this article can be found online at https://doi.org/10.1016/j.nme.2021.101106.

References

[1] S. Hémon, C.h. Dufour, F. Gourbilleau, E. Paumier, E. Dooryhée, S. Bégin-Colin, Influence of the grain size: yttrium oxide irradiated with swift heavy ions, Nucl. Instrum. Methods Phys. Res. B 146 (1-4) (1998) 443–448, https://doi.org/10.1016/S0168-583X(98)00479-0.

[2] S. Hémon, C. Dufour, A. Berthelot, F. Gourbilleau, E. Paumier, S. Bégin-Collin, Structural transformation in two yttrium oxide powders irradiated with swift molybdenum ions, Nucl. Instrum. Methods Phys. Res. B 166 (2000) 339–344, https://doi.org/10.1016/S0168-583X(99)00693-X.

[3] V. Grover, R. Shukla, R. Kumari, B.P. Mandal, P.K. Kulriya, S.K. Srivastava, S. Ghosh, A.K. Tyagi, D.K. Avasthi, Effect of grain size and microstructure on radiation stability of CeO₂: an extensive study, Phys. Chem. Chem. Phys. 16 (48) (2014) 27065–27073, https://doi.org/10.1039/C4CP04215H.

[4] W.F. Cureton, R.I. Palomares, J. Walters, C.L. Tracy, C.H. Chen, R.C. Ewing, G. Baldinozzi, J. Lian, C. Trautmann, M. Lang, Grain size effects on irradiated CeO₂, ThO₂, and UO₂, Acta Materialia 160 (2018) 47–56, https://doi.org/10.1016/j.actamat.2018.08.040.

[5] P. Kalita, S. Ghosh, G. Gutierrez, P. Rajput, V. Grover, G. Sattonnay, D.K. Avasthi, Grain size effect on the radiation damage tolerance of cubic zirconia against simultaneous low and high energy heavy ions: Nano triumphs bulk, Sci. Rep. 11 (2021) 1–10, https://doi.org/10.1038/s41598-021-90214-6.

[6] W.F. Cureton, C.L. Tracy, M. Lang, Review of Swift Heavy Ion Irradiation Effects in CeO₂, Quantum Beam Sci. 5 (2021) 19, https://doi.org/10.3390/qubs5020019.

[7] R.I. Palomares, C.L. Tracy, F. Zhang, C. Park, D. Popov, C. Trautmann, R.C. Ewing, M. Lang, In situ defect annealing of swift heavy ion irradiated CeO₂ and ThO₂ using synchrotron X-ray diffraction and a hydrothermal diamond anvil cell, J. Appl. Crystallogr. 48 (2015) 711–717, https://doi.org/10.1107/S160057671500477X.

[8] F. Lu, J. Wang, M. Lang, M. Toulemonde, F. Namavar, C. Trautmann, J. Zhang, R.C. Ewing, J. Lian, Amorphization of nanocrystalline monoclinic ZrO₂ by swift

heavy ion irradiation, Phys. Chem. Chem. Phys. 14 (2012) 12295–12300, https://doi.org/10.1039/C2CP41553D.

[9] S. Hemon, F. Gourbilleau, C.h. Dufour, E. Paumier, E. Dooryhee, A. Rouanet, TEM study of irradiation effects on tin oxide nanopowder, Nucl. Instrum. Methods Phys. Res. B 122 (3) (1997) 526–529, https://doi.org/10.1016/S0168-583X(96)00580-0.

[10] A. Berthelot, S. Hémon, F. Gourbilleau, C. Dufour, E. Dooryhée, E. Paumier, Nanometric size effects on irradiation of tin oxide powder, Nucl. Instrum. Methods Phys. Res. B 146 (1-4) (1998) 437–442, https://doi.org/10.1016/S0168-583X(98)00517-5.

[11] A. Berthelot, F. Gourbilleau, C. Dufour, B. Domenges, E. Paumier, Irradiation of a tin oxide nanometric powder with swift heavy ions, Nucl. Instrum. Methods Phys. Res. B 166 (2000) 927–932, https://doi.org/10.1016/S0168-583X(99)00732-6.

[12] N.J. Shivaramu, B.N. Lakshminarasappa, K.R. Nagabhushana, F. Singh, Ion beam induced cubic to monoclinic phase transformation of nanocrystalline yttria, Nucl. Instrum. Methods Phys. Res. B 379 (2016) 73–77, https://doi.org/10.1016/j.nimb.2016.04.013.

[13] M.-L. Lescoat, I. Monnet, J. Ribis, P. Dubuisson, Y. de Carlan, J.-M. Costantini, J. Malaplate, Amorphization of oxides in ODS materials under low and high energy ion irradiations, J. Nucl. Mater. 417 (1-3) (2011) 266–269, https://doi.org/10.1016/j.jnucmat.2011.01.065.

[14] J. Ribis, M.-L. Lescoat, Y. de Carlan, J.-M. Costantini, I. Monnet, T. Cozzika, F. Delabrouille, J. Malaplate, Stability of nano-oxides upon heavy ion irradiation of an ODS material, J. Nucl. Mater. 417 (1-3) (2011) 262–265, https://doi.org/10.1016/j.jnucmat.2010.12.068.

[15] I. Monnet, C. Grygiel, M.L. Lescoat, J. Ribis, Amorphization of oxides in ODS steels/materials by electronic stopping power, J. Nucl. Mater. 424 (1-3) (2012) 12–16, https://doi.org/10.1016/j.jnucmat.2012.01.026.

[16] V.A. Skuratov, V.V. Uglov, J. O'Connell, A.S. Sohatsky, J.H. Neethling, S.V. Rogozhkin, Radiation stability of the ODS alloys against swift heavy ion impact, J. Nucl. Mater. 442 (1-3) (2013) 449–457, https://doi.org/10.1016/j.jnucmat.2013.07.017.

[17] V.A. Skuratov, A.S. Sohatsky, J.H. O'Connell, K. Kornieieva, A.A. Nikitina, J.H. Neethling, V.S. Ageev, Swift heavy ion tracks in Y₂Ti₂O₇ nanoparticles in EP450 ODS steel, J. Nucl. Mater. 456 (2015) 111–114, https://doi.org/10.1016/j.jnucmat.2014.09.034.

[18] V.A. Skuratov, A.S. Sohatsky, J.H. O'Connell, K. Kornieieva, A.A. Nikitina, J.H. Neethling, V.S. Ageev, M. Zdorovets, A.D. Volkov, Stability of Y-Ti-O nanoparticles in ODS alloys during heat treatment and high temperature swift heavy ion irradiation, Phys. Status Solidi C 13 (10-12) (2016) 927–931, https://doi.org/10.1002/pssc.201600080.

[19] V.A. Skuratov, A.S. Sohatsky, J.H. O'Connell, K. Kornieieva, A.A. Nikitina, J.H. Neethling, V.S. Ageev, Latent Tracks of Swift Heavy Ions in Cr₂₃C₆ and Y-Ti-O Nanoparticles in ODS Alloys, Nucl. Instrum. Methods Phys. Res. B 374 (2016) 102–106, https://doi.org/10.1016/j.nimb.2015.08.089.

[20] S.V. Rogozhkin, A.A. Bogachev, A.A. Nikitina, A.L. Vasiliev, M.Y. Presnyakov, M. Tomut, C. Trautmann, TEM analysis of radiation effects in ODS steels induced by swift heavy ions, Nucl. Instrum. Methods Phys. Res. B 486 (2021) 1–10, https://doi.org/10.1016/j.nimb.2020.10.017.

[21] M.S. Lehmann, A.N. Christensen, H. Fjellvåg, R. Feidenhans'l, M. Nielsen, Structure determination by use of pattern decomposition and the Rietveld method on synchrotron X-ray and neutron powder data; the structures of Al₂Y₄O₉ and I₂O₄, J. Appl. Crystallogr. 20 (1987) 123–129, https://doi.org/10.1107/S0021889887087016.

[22] M. Toulemonde, W. Assmann, C. Dufour, A. Meftah, F. Studer, C. Trautmann, Experimental phenomena and thermal spike model description of ion tracks in amorphisable inorganic insulators, Mat. Fys. Medd. 52 (2006) 263–292.

[23] R. Sachan, Y. Zhang, X. Ou, C. Trautmann, M.F. Chisholm, W.J. Weber, New insights on ion track morphology in pyrochlores by aberration corrected scanning transmission electron microscopy, J. Mater. Res. 32 (2016) 928–935.

[24] T. Kitayama, Y. Morita, K. Nakajima, K. Narumi, Y. Saitoh, M. Matsuda, M. Sataka, M. Tsujimoto, S. Isoda, M. Toulemonde, K. Kimura, Formation of ion tracks in amorphous silicon nitride films with MeV C₆₀ ions, Nucl. Instrum. Methods Phys. Res. B 356 (2015) 22–27, https://doi.org/10.1016/j.nimb.2015.04.051.

[25] R.A. Rymzhanov, N. Medvedev, J.H. O'Connell, A. Janse van Vuuren, V.A. Skuratov, A.E. Volkov, Recrystallization as the governing mechanism of ion track formation, Sci. Rep. 9 (2019) 1–10, https://doi.org/10.1038/s41598-019-40239-9.

[26] M.D. Rodriguez, W.X. Li, F. Chen, C. Trautmann, T. Bierschenk, B. Afra, D. Schauries, R.C. Ewing, S.T. Mudie, P. Kluth, SAXS and TEM investigation of ion tracks in neodymium-doped yttrium aluminium garnet, Nucl. Instrum. Methods Phys. Res. B 326 (2014) 150–153, https://doi.org/10.1016/j.nimb.2013.10.076 0168-583X.

[27] A. Janse van Vuuren, M.M. Saifulin, V.A. Skuratov, J.H. O'Connell, G. Aralbayeva, A. Dauletbekova, M. Zdorovets, The influence of stopping power and temperature on latent track formation in YAP and YAG, Nucl. Instrum. Methods Phys. Res. B 460 460 (2019) 67–73, https://doi.org/10.1016/j.nimb.2018.11.032.